J. Fluid Mech. (1979), *vol.* 95, *part* 2, *pp.* 347–367
Printed in Great Britain

The laminar horseshoe vortex

By C. J. BAKER
Cambridge University Engineering Department

(Received 13 November 1978)

The horseshoe vortex formed around the base of a cylinder by a separating laminar boundary layer has been investigated experimentally. Smoke flow visualization shows that both steady and unsteady vortex systems exist. Pressure distributions beneath both types of vortex system have been measured and the variation of the horseshoe vortex position on the plane of symmetry upstream of the cylinder has been determined. Unsteady horseshoe vortex systems are shown to have a complex oscillatory behaviour and the nature of this oscillatory behaviour is described. Using smoke flow visualization techniques some measurements have been made of the velocity distributions within horseshoe vortex systems.

1. Introduction

If a cylinder is placed on a wall over which there is a fluid flow with its axis perpendicular to the wall, this cylinder produces pressure gradients in its vicinity. The boundary layer on the wall upstream of the cylinder is in a region of adverse pressure gradient and some distance upstream of the cylinder this boundary layer will undergo a three-dimensional separation. The separated boundary layer rolls up downstream of the separation line to form a system of vortices. This vortex system is swept around the base of the cylinder and assumes a characteristic shape which has led to its name – the horseshoe vortex. Such a system is shown in figure 1 (plate 1) [taken by E. P. Sutton and printed in Thwaites (1960)] on the plane of symmetry ahead of a 7·6 cm diameter cylinder, 3·8 cm in height. The flow is from left to right and the vortex system is made visible by filaments of smoke injected into the flow. Several vortices are visible upstream of the cylinder. Such a vortex system is formed by a separating laminar boundary layer, but similar systems are formed by separating turbulent boundary layers.

Such flows exist in many situations. For example a horseshoe vortex system will be formed at the junction of an aeroplane wing with the fuselage. Such a system will also form at the junction of plate and support in a plate heat exchanger. A horseshoe vortex system will produce high wall shear stresses beneath it, and if such a system is formed around an obstacle on an erodible bed (for example, around a bridge pier in the sand bed of a river), these high shear stresses will cause the bed to be eroded and a scour hole to form around the base of the obstacle. This effect may also be seen around a telegraph pole surrounded by a snowdrift.

A considerable amount has been written about the various aspects of horseshoe vortex systems. A complete literature review is not presented here, and the interested reader is referred to Baker (1978). [This paper, in fact, reports some of the findings of the experimental investigation of Baker (1978), who discusses, in some detail, turbulent horseshoe vortices and scour around bridge piers in a river bed.] However, one previous

0022–1120/79/4310–7630 $02.00

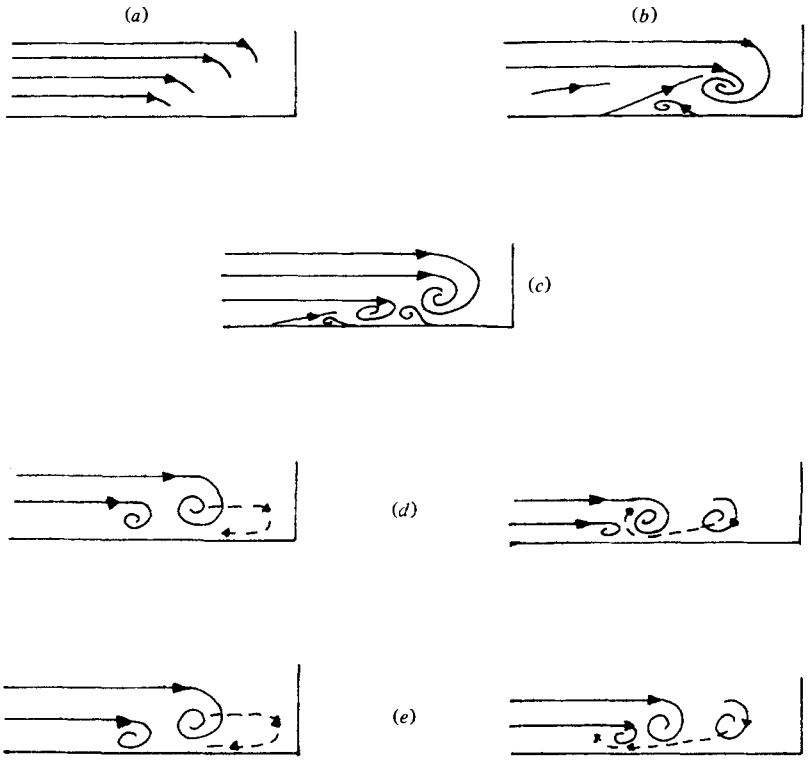

FIGURE 2. Schwind's experiment: (*a*) regime 1; (*b*) regime 2; (*c*) regime 3; (*d*) regime 4; (*e*) regime 5.

experimental investigation will be described here; that of Schwind (1962). For this investigation a specially built low speed wind tunnel was used, and laminar horseshoe vortices were observed in front of a 60° wedge which divided the wind tunnel into two. Very detailed observations were made of the flow using smoke introduced into the flow upstream of the wedge, for speeds between 0·16 m s^{-1} and 1·33 m s^{-1}. Schwind observed five types of vortex regimes (figure 2). At the lowest speeds used he observed flow of the 'regime 1' type, which he described as 'a steady separation with no vortices visible'. This description seems a little misleading. If the flow does separate upstream of the wedge, then downstream of the separation line, there will be a flow in the upstream direction, which implies some form of vortex behaviour. Perhaps it would be more correct to say that in 'regime 1' type flow only a very weak, slowly rotating vortex is formed, that is observable only on the plane of symmetry. As the flow velocity was increased, flow of the 'regime 2' type was observed, with a single steady clockwise rotating vortex and a small triangular-shaped counter-rotating vortex visible. The need for velocity gradients to be continuous implies that a second vortex rotating in the same direction as the main vortex must be present upstream of the small counter-rotating vortex, although this was not observed by Schwind for flows of the regime 2 type. When such a vortex was observed Schwind defined this as 'regime 3' type flow, which appeared as the velocity increased. A second small counter-rotating vortex was also observed in this type of flow. As the velocity was further increased the two clockwise rotating vortices were seen to start to oscillate, the amplitude increasing with the velocity. In flows of 'regime 4' and 'regime 5' types, which occurred at yet higher

velocities, regular oscillatory motion was observed with the main vortex apparently becoming isolated from the rest of the vortex system and moving towards the wedge, then moving back upstream. For 'regime 4' type flow the vortex was seen to combine with the second vortex, while for 'regime 5' type flow it was seen to pass beneath the second vortex. Since this vortex could not pass out of the separated region it presumably combined with an unobserved third clockwise rotating vortex.

Schwind pointed out that, although the flow passed from regime 1 to regime 5 types as the velocity increased, the velocity at which the flow changed from one regime to another was by no means well defined and different flow regimes could exist at one velocity. From pulsed smoke observations, Schwind obtained some not very accurate measurements of the velocity within the horseshoe vortex system, for steady vortex systems. From ciné film analysis he obtained much information on how the vortex position changed with time for unsteady systems, both on and off the plane of symmetry. He also attempted to find how the vortex position varied with the various flow parameters, and how the oscillation frequency varied for unsteady systems. However, he met with little success.

In the experiments described in this paper extensive flow visualization experiments were carried out to describe in detail the flow upstream of circular cylinders mounted on a wall on which a laminar boundary layer is growing, with its axis perpendicular to the wall. Both steady and oscillating vortex systems were observed. Pressure distributions were measured on the plane of symmetry upstream of the cylinders. The nature of the oscillating vortex systems was investigated in some detail. Measurements of the velocity distributions within the vortex systems were also made.

In this paper a Cartesian co-ordinate system (x, y, z) will be used: x, the streamwise co-ordinate, is measured from the origin (at the intersection of the cylinder axes and the wall on which the cylinders are mounted) in a downstream direction; y is measured from the origin in a direction perpendicular to the wall; z is measured from the origin in a direction which is consistent with the directions of x and y and the right-hand rule. The velocities in the x, y and z directions are u, v and w respectively.

2. Dimensional analysis

If, in a horseshoe vortex system around an obstacle formed by the separation of an incompressible laminar boundary layer, x_v is the distance from the obstacle centre to the centre of the vortex core on the plane of symmetry, then one may write

$$x_v = \text{fn}\,(D, l, U, \delta^*, H, u_y', \mu, \rho), \tag{2.1}$$

where D is the obstacle diameter and l the obstacle height. U is the freestream fluid velocity, and δ^* and H are, respectively, the boundary-layer displacement thickness and form parameter at the obstacle position when the obstacle is not in position. u_y' is the distribution of turbulence within the oncoming boundary layer, and μ and ρ are the fluid viscosity and density respectively.

Non-dimensionalizing (2.1) gives

$$\frac{x_v}{D} = \text{fn}\left(\frac{UD}{\nu}, \frac{D}{l}, \frac{D}{\delta^*}\, H, \frac{u_y'}{U}\right), \tag{2.2}$$

where $\nu (= \mu/\rho)$ is the kinematic viscosity.

Similarly if x_s is the distance from the obstacle centre to the separation line upstream of the obstacle on the plane of symmetry one may take x_s/D to be a function of the dimensionless groups of equation (2.2). Also it will be shown in §4 that for some values of the flow parameters horseshoe vortex systems exhibit regular oscillatory behaviour. If f is the frequency of such oscillations then one may also take the Strouhal number fD/U to be a function of the dimensionless groups of (2.2).

In the following sections the variation of the dependent dimensionless variables (x_v/D, x_s/D and fD/U) will be considered for several different obstacle shapes. For all the obstacles used D/l is small ($= 0{\cdot}21$ for the quantitative parts of the investigation, §§5, 6 and 7) and it will be assumed that the values of the dependent dimensionless variables do not depend on this dimensionless group. Also it will be seen that the form parameter H does not vary greatly (§3) and it will be assumed that such small variations do not affect the dependent dimensionless variables. Further the variations of the turbulence distribution throughout the boundary layer will not be considered. (It will be shown that the only significant variations in the turbulence distribution occur at the higher velocities used.)

Thus for a horseshoe vortex system caused by a separating laminar boundary layer we are left with

$$\frac{x_v}{D}, \frac{x_s}{D}, \frac{fD}{U} = \text{fn}\left(\frac{UD}{\nu}, \frac{D}{\delta^*}\right). \tag{2.3}$$

In the following sections the dependent dimensionless variables will be plotted in the UD/ν against D/δ^* plane.

3. Experimental apparatus

In this section only an outline of the experimental apparatus is given. Full details are given by Baker (1978).

(*a*) *Flow visualization.* Flow visualization was carried out in a smoke tunnel with a cross-section of 30·5 by 15·3 cm. A 7·6 cm diameter cylinder, 3·8 cm in height, was mounted on a flat plate on the centre-line of the tunnel working section. The values of the non-dimensional variables quoted for tests in this tunnel (§§4 and 8) should only be regarded as approximate because of wall interference effects [see Baker (1978)].

(*b*) *Pressure measurement.* Measurements of the pressure distribution upstream of a 6·35 cm diameter cylinder, 30·5 cm in height, were made with the cylinder mounted on the wall of Number 1 B Wind Tunnel (with a cross-section of 51 × 71 cm). The wind-tunnel wall boundary layer was removed through a suction slot inserted into the wind-tunnel wall upstream of the cylinder. A laminar boundary layer therefore grew on the wind-tunnel wall between the suction slot and the model. By placing the cylinder and suction slot at different positions relative to one another, the cylinder could be positioned in regions of different boundary-layer characteristics. How these characteristics vary with the tunnel speed at the various suction slot positions used is shown in figure 3. It can be seen that the form parameter H is approximately equal to the value for boundary-layer growth on a flat plate in zero pressure gradient (2·59), to within experimental error. Also it was found that the turbulence level within the boundary layer did not exceed 1 % of the freestream velocity except at the higher speeds used (over 3 m s^{-1}).

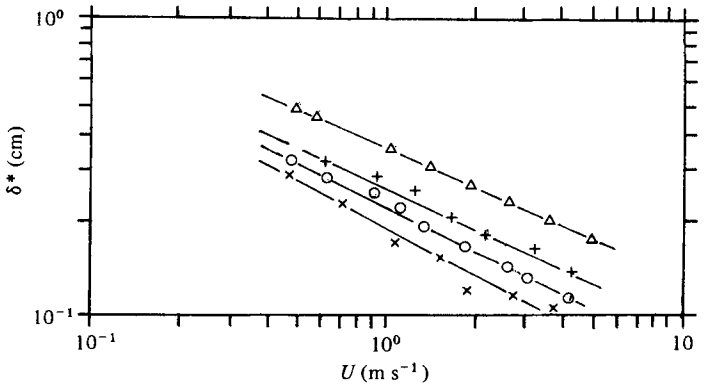

FIGURE 3. Boundary-layer characteristics. ×, Suction slot position 1, $H = 2{\cdot}56$; ○, suction plot position 2, $H = 2{\cdot}69$; +, suction slot position 3, $H = 2{\cdot}61$; △, suction plot position 4, $H = 2{\cdot}79$.

The pressure on the plane of symmetry upstream of the cylinder was measured successively at each of six pressure tappings, placed 2 cm apart. The cylinder could be traversed 2 cm along the wind tunnel wall, so a continuous pressure distribution could be obtained.

(*c*) *Measurements of vortex oscillations.* These experiments were again conducted on the wall of 1 B Wind Tunnel, upstream of the 6·35 cm diameter cylinder. DISA hot-wire '*u*' probes were inserted through a small hole in the wind tunnel wall beneath the horseshoe vortex system, so that the tips of the probes just extended into the flow. DISA bridges and linearizers were used to analyse the signals from the probes, which were recorded on a Racal T3000 tape recorder. Spectral analyses were carried out on the Cambridge University Engineering Department's 'α' mini-computer.

(*d*) *Velocity measurements.* Velocity measurements were made upstream of a 7·6 cm diameter cylinder, 3·8 cm in height, mounted on a plate in the smoke tunnel. Smoke filaments were filmed at 64 frames per second as they entered the horseshoe vortex system. A frame-by-frame analysis of the films was then carried out and, by measuring the difference in position of the ends of the smoke filament between successive frames, the flow velocity within nearly all the regions of the vortex system could be determined.

4. Flow visualization results

4.1. *General description of horseshoe vortex flows*

Figure 1, taken from Thwaites (1960), shows a photograph taken by E. P. Sutton in the smoke tunnel used for flow visualization experiments in this investigation. It shows the flow pattern on the plane of symmetry upstream of a short cylinder on a plate, formed by the separation of a laminar boundary layer. The reflexion of this flow pattern in the plate can also be seen.

Figure 1 is typical of the flow patterns seen in the smoke tunnel at the lower speeds used. There are at least three vortices rotating in the clockwise direction and two smaller vortices rotating in the opposite direction. The exact number of vortices was seen to depend upon the flow speed and cylinder size, more vortices appearing as the speed increased. With a 7·62 cm diameter cylinder in the tunnel, above a certain flow speed (approximately 0·65 m s^{-1}) the entire horseshoe vortex system began to oscillate

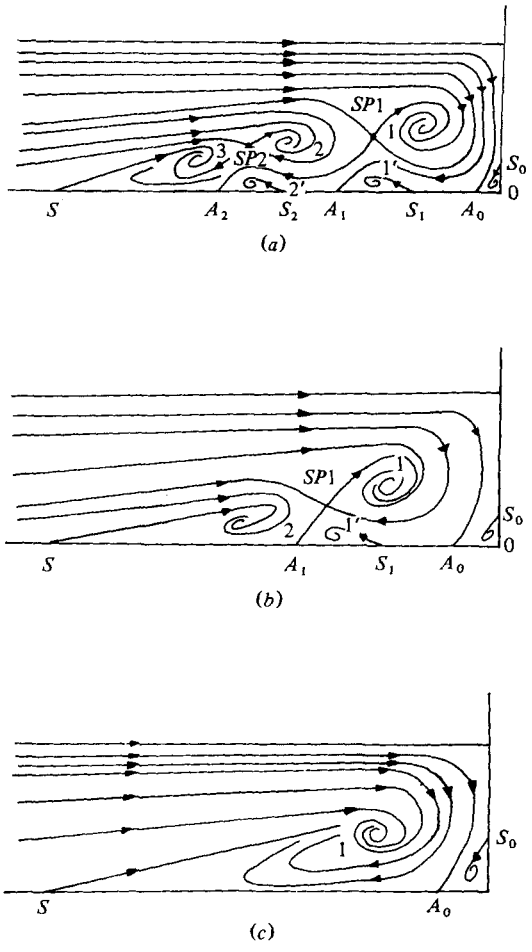

FIGURE 5. Streamline patterns: (*a*) Six vortex system; (*b*) four vortex system; (*c*) two vortex system. *S*, separation line; *A*, attachment line; *SP*, stagnation point.

in a regular manner with the two largest clockwise rotating vortices moving towards one another and apart again. At higher speeds (above approximately 0·8 m s^{-1}) the largest clockwise rotating vortex ceased to be fed by smoke during part of the oscillation period and seemed to become detached from the rest of the vortex system. At still higher speeds (above approximately 1·4 m s^{-1}) the flow appeared to be very unsteady and turbulent and showed no traces of periodicity. These steady and oscillating horseshoe vortex systems will be discussed in more detail in the following sections.

4.2. *Detailed description of steady horseshoe vortices*

Consider the horseshoe vortex system that is shown in the photographs of figure 4 (plate 2). The filament of smoke that feeds into the vortex system is being moved closer to the plate on which the cylinder is mounted as we proceed from figure 4 (*a*) to figure 4 (*g*). When the filament just begins to flow into the vortex system, it flows into a small anticlockwise rotating vortex formed by separation of the flow from the face

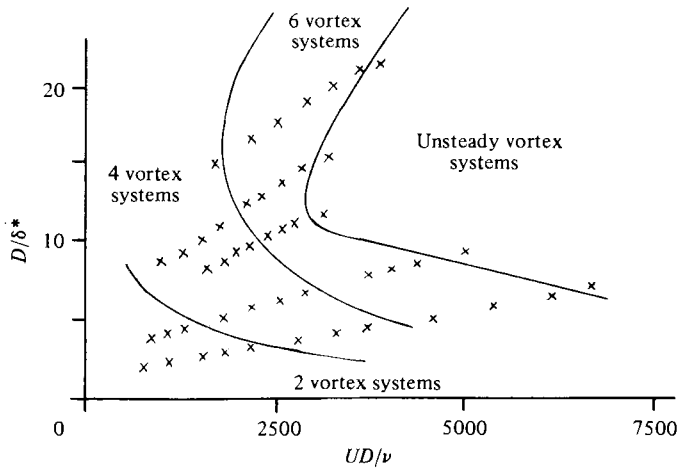

FIGURE 6. Variation in vortex number (× indicates the position of experimental observation in UD/ν, D/δ^* plane). $D/l = 2{\cdot}0$.

of the cylinder. The smoke filament passes around the base of the cylinder (figure 4*a*). We will call this vortex 'vortex 0'.

As the smoke filament moves closer to the plate, it flows down the face of the cylinder, then along the plate away from the cylinder and into a small triangular vortex. This vortex assumes a horseshoe shape around the side of the cylinder. We will call this vortex (for reasons that will become apparent later) 'vortex 1'' (figure 4*b*).

As the smoke filament moves still closer to the plate, it flows away from the cylinder, over vortex 1' and into a small flattened vortex rotating in the same direction as vortex 1'. We will call this vortex 'vortex 2'' (figure 4*c*).

As the movement of the smoke filament continues, the smoke flows into a large vortex, rotating in a clockwise direction and situated between vortex 1' and the cylinder. This vortex will be referred to as 'vortex 1', or the primary vortex (figures 4*d* and 4*e*).

With the smoke filament still closer to the plate, the smoke flows into two further vortices rotating in the same direction as vortex 1. The one closer to the cylinder will be referred to as 'vortex 2', the one further away as 'vortex 3' (figures 4*f* and 4*g*).

The order of 'feeder layers' for vortices 2 and 3 is not very clear from the photographs but it appears from these figures that as the smoke filament moves towards the plate vortex 3 is fed first, then vortex 2 and when the smoke filament is right next to the surface of the plate vortex 3 is fed once more. The streamline pattern that can be inferred from these photographs is shown in figure 5(*a*).

This type of vortex system is an example of a six vortex system, which was the most complex system observed in the smoke tunnel. Four and two vortex systems were also observed under different flow conditions and the streamline patterns observed are shown in figures 5(*b*) and 5(*c*). Also in this figure the various separation lines (S, S_0, S_1, S_2), attachment lines (A_0, A_1, A_2) and free stagnation points (SP1, SP2) are shown.

Figure 6 shows how the number of vortices varies with the flow parameters, determined from observations around cylinders of various sizes. (The value of δ^* was calculated from the Blasius formula.) It can be seen that the number of vortices that were observable increases as UD/ν and D/δ^* increase.

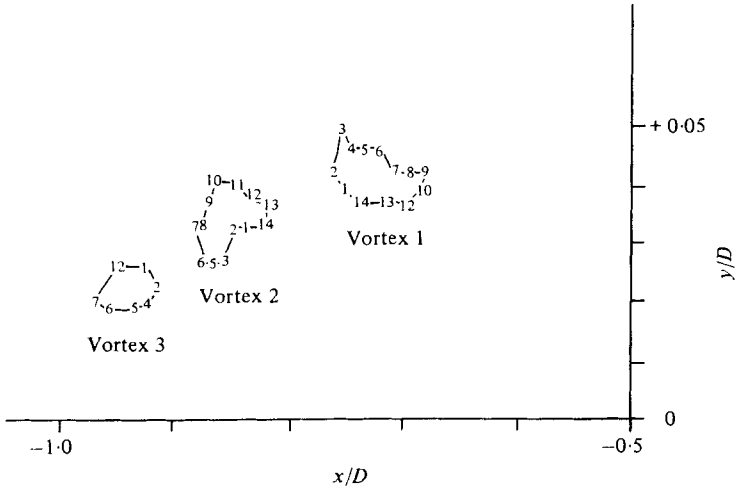

FIGURE 8. Variation of vortex position (from figure 7, plate 3).

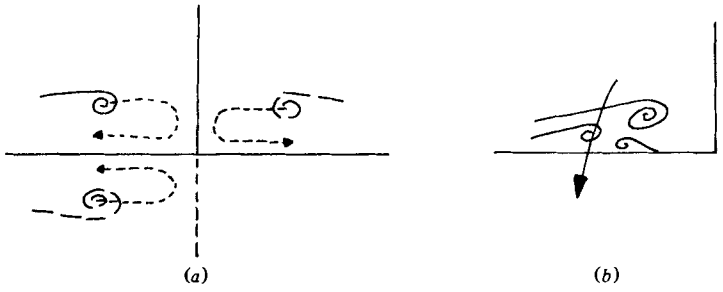

FIGURE 9. Potential vortex approximation: (*a*) image systems; (*b*) the influence of vortex 1′ on vortex 2.

4.3. *Detailed description of oscillating horseshoe vortex systems*

In this section the photographs of an oscillating horseshoe vortex system shown in figure 7 (plate 3) will be considered. In these photographs, taken from a positive ciné film, smoke appears black against a white background. The primary vortex (1) initially moves towards the cylinder (frames 1 to 9) and the smoke filament to it is cut so it appears to become isolated. Then it moves back upstream and entrains smoke from the outer layers of the secondary vortex (2) (frames 10 to 14) until the initial flow pattern is re-established. It is not possible to determine whether vortex 1 does cease to be fed by any fluid as it moves towards the cylinder, or whether the smoke filament is cut and vortex 1 simply seems to become isolated.

The paths taken by vortices 1, 2 and 3 during one oscillation are shown in figure 8. It is instructive to consider the vortex system to consist of potential vortices and their images (in a manner similar to Schwind (1962)) and to analyse the movements of figure 5 in this light (figure 9*a*). As vortex 1 is convected downstream (frames 1 to 9) it becomes influenced to a greater extent by its image in the cylinder and thus moves down towards the plate. As it moves closer to the plate it becomes influenced more and more by its image in the plate and thus moves back upstream where it entrains the outer layers of vortex 2 (frames 10 to 14).

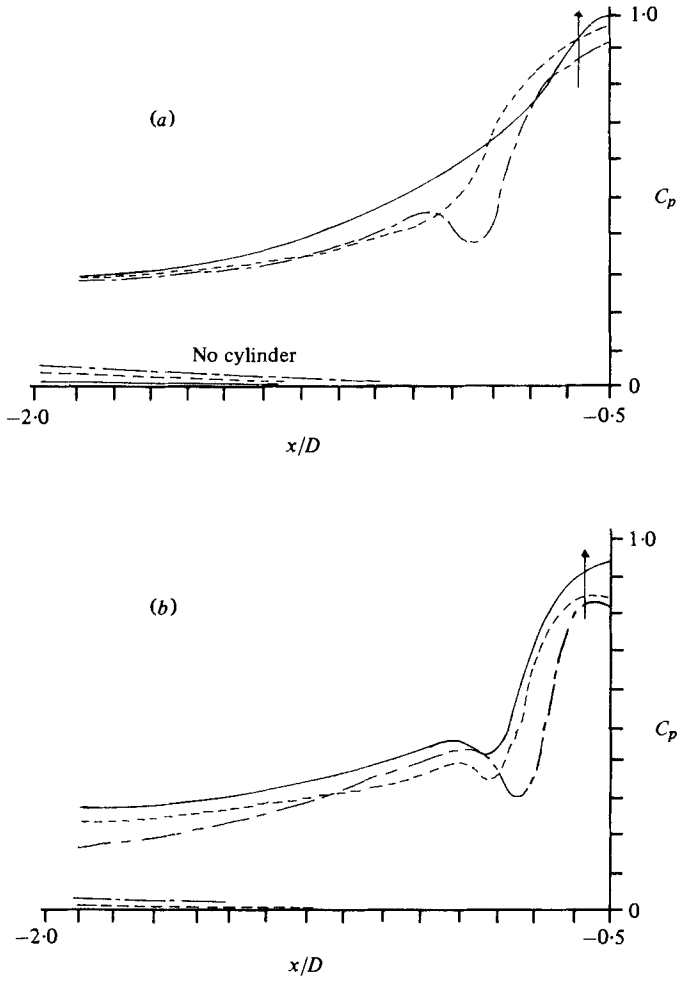

FIGURE 10. Pressure distributions on plane of symmetry upstream of cylinders. (*a*) ——, UD/ν = 16 130, D/δ^* = 65·8; – – –, UD/ν = 7890, D/δ^* = 44·6; — — —, UD/ν = 4790, D/δ^* = 33·8. (*b*) ——, UD/ν = 3840, D/δ^* = 30·5; – – –, UD/ν = 2940, D/δ^* = 26·3; — — —, UD/ν = 2050, D/δ^* = 21·7. The arrow indicates UD/ν, D/δ^* increasing as the boundary layer thins.

As vortex 1 moves towards the cylinder vortex 1′ must move with it, since it is caused by separation under vortex 1. Since the effect of vortex 1′ on vortex 2 is to pull it down onto the plate (figure 9*b*) when vortex 1′ moves away from vortex 2, vortex 2 rises from the plate (frames 3 to 10). In a similar manner when vortex 1 (and hence vortex 1′) moves back towards vortex 2, vortex 1′ influences vortex 2 to a greater extent and vortex 2 moves back towards the plate (frames 11 to 14).

The oscillating flow described above is very similar to the 'regime 4' flow of Schwind (§1). However, it was not possible to observe Schwind's 'regime 5' flow. As the tunnel speed was increased above approximately 1·4 m s^{-1} (with a 7·62 cm diameter cylinder) the horseshoe vortex system appeared to become turbulent and no regular oscillatory motion could be seen.

5. Plane of symmetry pressure measurements

In this section pressure distributions on the plane of symmetry upstream of the 6·35 cm diameter cylinder mounted on the wall of the 51 × 71 cm tunnel will be presented. The pressure coefficient used in this section (C_p) is based upon the velocity and pressure at the model position without the model being in position. The pressure distributions (figure 10) are tracings of chart recorder outputs. It can be seen that there are two types of distribution. For $UD/\nu < 5000$, the curves have minima, while for $UD/\nu > 5000$ no minima can be seen. Similar measurements were made upstream of a cylinder mounted on a plate in the smoke tunnel, and were accompanied by flow visualization experiments. These experiments showed that the minima in the pressure distributions were at the position of the primary vortex. When the pressure distributions do not show minima, then the flow visualization showed that unsteady vortex systems existed. So for $UD/\nu < 5000$, steady vortex systems exist, and the position of the primary vortex can be determined from plane of symmetry pressure distributions. The variation of this vortex position with the flow parameters will be discussed in §6. For $UD/\nu > 5000$, unsteady vortex systems exist.

At the model leading edge ($x/D = -0{\cdot}5$) C_p is below 1·0. It can be seen that as UD/ν and D/δ^* increase C_p at $x/D = -0{\cdot}5$ also increases. This can be explained in the following manner. As the flow variables change, the vertical dimensions of the vortex system do not change significantly. (For example, for $D/l = 2{\cdot}0$, the free stagnation point SP1 was found to have a value of y/D of $0{\cdot}072 \pm 0{\cdot}005$ at all flow velocities, and one of the streamlines that approached it was found to have an upstream value of y/D of $0{\cdot}115 \pm 0{\cdot}005$.) Thus as UD/ν or D/δ^* increases and the boundary layer becomes thinner, then the fluid that passes close to the upstream edge of the cylinder will come from a region of higher non-dimensional velocity. Now C_p at $x/D = -0{\cdot}5$ is given by

$$C_p(x/D = -0{\cdot}5) = \frac{(p(x/D = -0{\cdot}5) - p_0)}{\frac{1}{2}\rho U_0^2}, \tag{5.1}$$

where the subscript 0 refers to conditions at the model position without the model being in position. Now $p(x/D = -0{\cdot}5)$ is approximately equal to the stagnation pressure on the streamline passing down the face of the cylinder

$$p(x/D = -0{\cdot}5) = p_\infty + \tfrac{1}{2}\rho u_\infty^2, \tag{5.2}$$

where p_∞ is the pressure far upstream and U_∞ is the velocity on that particular streamline far upstream. If one assumes that $p_0 \approx p_\infty$ and $U_0 \approx U_\infty$ then we have

$$C_p(x/D = -0{\cdot}5) \approx (u_\infty/U_\infty)^2. \tag{5.3}$$

So as the dimensionless velocity on the streamline passing down the face of the cylinder increases (i.e. as UD/ν and D/δ^* increase) then $C_p(x/D = -0{\cdot}5)$ will also increase.

Also shown in figure 10 are the pressure distributions measured without the model in position. It can be seen that the models are in a region of slightly favourable pressure gradient.

Figure 11 shows pressure distributions ahead of the cylinder, obtained with the suction slot in positions 1, 2 and 3. These show the variation in the pressure distribution

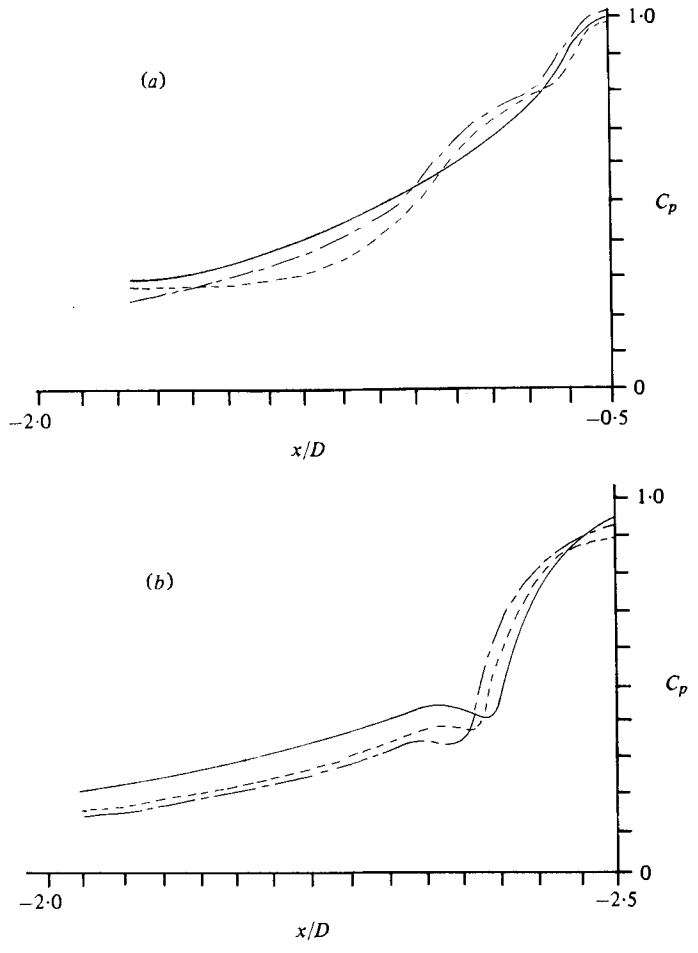

FIGURE 11. Pressure distributions on plane of symmetry upstream of cylinder at different suction slot positions. (*a*) ——, $UD/\nu = 16130$, $D/\delta^* = 65{\cdot}8$; – – –, $UD/\nu = 15710$, $D/\delta^* = 52{\cdot}6$; — — —, $UD/\nu = 15380$, $D/\delta^* = 42{\cdot}4$. (*b*) ——, $UD/\nu = 3840$, $D/\delta^* = 30{\cdot}5$; – – –, $UD/\nu = 8710$, $D/\delta^* = 25{\cdot}0$; — — —, $UD/\nu = 3720$, $D/\delta^* = 21{\cdot}7$.

as D/δ^* varies. The distributions for an oscillatory type of flow show little variation, but, where the vortex position can be distinguished, it can be seen that the vortex moves away from the model as D/δ^* decreases.

6. Variation of the horseshoe vortex position

Figure 12 shows how x_v/D, the dimensionless vortex position, varies upstream of the cylinder. Contours of x_v/D are plotted in the $UD/\nu - D/\delta^*$ plane as suggested by the dimensional analysis of § 2. The values of x_v/D were obtained from pressure distributions with the suction slot in all four positions. The dotted lines in the figures join experimental points corresponding to one suction slot position. The positions of the experimental points in figure 9 are at the position of the 'decimal points' of the values of x_v/D. The possible error in x_v/D indicated on figure 12 is considerable since it was not possible to determine accurately the position of the minima in the pressure distri-

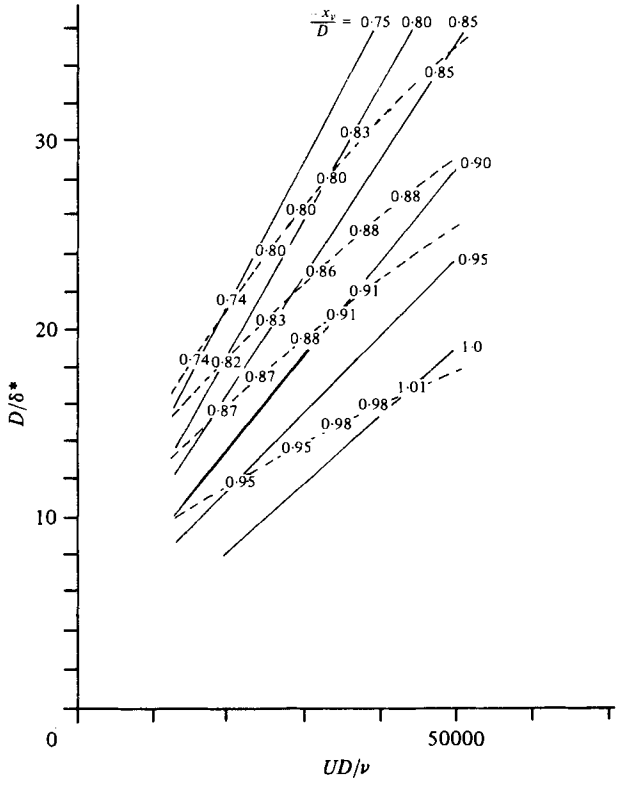

FIGURE 12. Variation of distance of vortex 1 from cylinder centre (x_v/D) (error in $x_v/D \simeq 0{\cdot}03$).

butions. It can be seen from this figure that, as UD/ν increases, x_v/D increases and, as D/δ^* increases, x_v/D decreases. No pressure minima were observed for values of UD/ν above approximately 5000, and the flow visualization suggests that when UD/ν is above this value oscillating vortex systems exist.

Experiments were carried out to determine how the separation position upstream of the cylinder varied as the flow parameters varied, since it was thought possible that this separation position might determine the vortex position. Smoke was let into the flow through a hole in the base of the cylinder and the separation position was taken as being the extreme upstream position to which the smoke penetrated. It was found that, for each suction slot position, the separation position remained constant as the tunnel speed varied. Thus if the separation position fixes the vortex position, then one would expect that the vortex position would not change along the dottted lines in figure 12. This can be seen not to be the case, so the vortex position is not fixed solely by the separation position but some other effect plays a part. What this effect may be has not been determined.

Baker (1978) shows, using the laminar boundary-layer calculation method of Timman (1955), that the dimensionless separation position (x_s/D) upstream of a cylinder on a flat plate depends only upon the dimensionless distance from the cylinder centre to the plate leading edge (i.e. x_0/D). x_s/D was found to increase as x_0/D increased. It can be seen from figure 12 that as D/δ^* decreases, at fixed UD/ν, x_v/D increases.

Now for the case of a cylinder on a flat plate (from the Blasius velocity distribution)

$$\frac{x_0}{D} = 0{\cdot}33\left(\frac{UD}{\nu}\right)\left(\frac{\delta^*}{D}\right)^2.$$

So at constant UD/ν a reduction in D/δ^* is equivalent to an increase in x_0/D, and, as stated above, an increase in x_0/D leads to an increase in x_s/D. Thus as D/δ^* decreases, x_s/D will increase. If one assumes that the horseshoe vortex position is largely determined by the separation position, then it is to be expected that x_v/D will also increase, as is seen to be the case.

7. The oscillatory behaviour of horseshoe vortex systems

To study the oscillatory behaviour of horseshoe vortex systems, a hot-wire probe was placed in the flow so that its wire was 1 mm from the wind tunnel wall, with the suction slot in position 1. Flow visualization suggests that with the probe in this position the flow was not affected. The hot-wire output was recorded at several velocities and spectral analyses were carried out. The spectra obtained were not repeatable, the number and magnitude of peaks in the spectra at any one velocity varying from run to run. The hot-wire output was then displayed on a storage oscilloscope and the situation was clarified. At any one speed four different waveforms could be seen at different times:

(*a*) a steady trace with no oscillations;

(*b*) a low frequency oscillation ($St = fD/U = 0{\cdot}26$);

(*c*) a high frequency oscillation ($St = 0{\cdot}40$, increasing to about 0·60 at higher UD/ν);

(*d*) an irregular turbulent trace.

Each of the above four states might exist for any length of time between 1 second and 5 minutes and the flow switched from one state to another in a completely random manner. At the lowest speeds used, state (*a*) was observed more often than the other states, but as the velocity increased state (*b*) became the most often observed state. As the velocity was increased further state (*c*) was observed more often and at the highest speeds only a turbulent trace (state (*d*)) could be seen.

After many attempts tape recordings were made of signals of just one of the above states, of sufficient length to enable a spectral analysis to be carried out. The spectra obtained are shown in figures 13(*a*) and 13(*b*). Here $\bar{P}$ is the dimensionless power spectral density. Note that the flow parameters are almost identical in both cases, but the peaks occur at completely different frequencies. In figure 13(*a*) for the dominant peak, $St = 0{\cdot}26$, and in figure 13(*b*) for the dominant peak, $St = 0{\cdot}36$. The smaller peaks in both spectra are harmonics of the main peaks. They appear simply because of the shape of the waveform of the hot-wire output, which is in turn dependent upon the exact position of the hot-wire probe in the flow.

Further tests were carried out with the suction slot at positions 2, 3 and 4. With the suction slot at position 2, the unsteady behaviour was similar to that described above, but with the suction slot at position 3 the lower frequency oscillations were seen only very occasionally. With the suction slot at position 4 no regular oscillatory motion was observed. With the slot at this position the periods of steady flow were observed at much higher velocities than for suction slot positions 1 to 3. These periods of steady

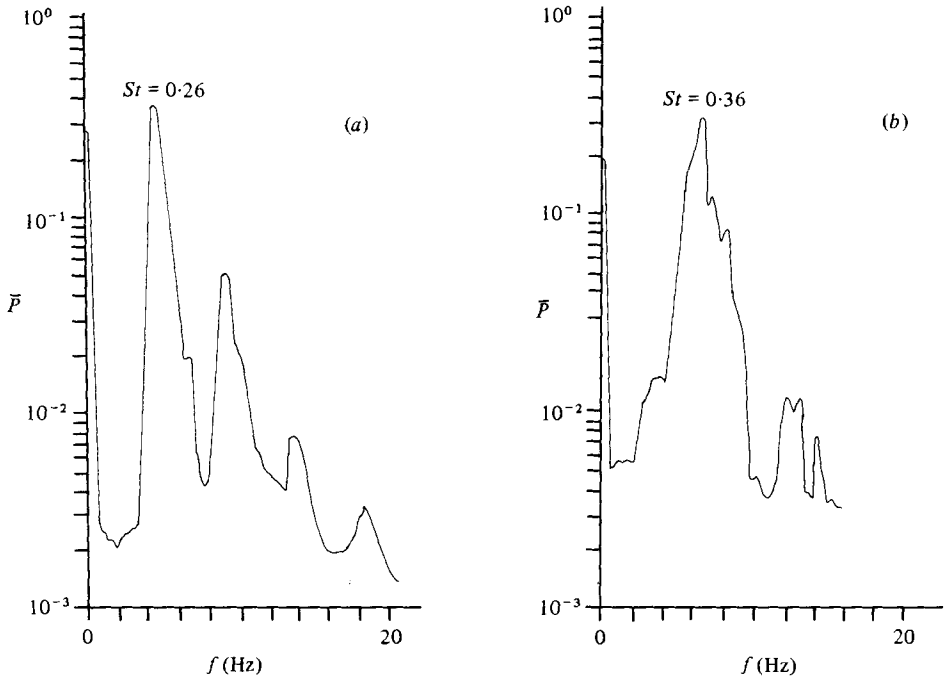

FIGURE 13. Horseshoe vortex spectra ($x/D = -0{\cdot}82$, $y/D = 0{\cdot}063$, $z/D = 0$). (*a*) $UD/\nu = 4720$, $D/\delta^* = 33{\cdot}8$; (*b*) $UD/\nu = 4780$, $D/\delta^* = 34{\cdot}2$.

flow were interrupted by bursts of irregular turbulent flow. These bursts of turbulent flow were probably caused by bursts of turbulence in the upstream boundary layer passing into the vortex system.

The variation of Strouhal number with the flow parameters for both types of oscillation is shown in figure 14. The frequencies were measured by displaying the hot-wire output on a storage oscilloscope and measuring the distance between adjacent peaks in the waveform, from many different output traces, and taking the average distance between peaks to be a measure of the oscillation period. It can be seen from figure 11 that for the high frequency oscillation (the 'primary' oscillation) St increases as UD/ν increases, while for the low frequency oscillation (the 'secondary' oscillation) St remains fairly constant. (There was a considerable variation in the oscillation frequency at any one set of flow conditions as can be judged from the width of the dominant peak in the spectra of figure 10.)

Schwind (1962), as stated in § 1, observed two types of oscillation (figure 2). At a speed of 0·45 m s^{-1} he measured a frequency of oscillation of 0·8 Hz for flows of the regime 4 type and a frequency of 1·4 Hz for flows of the regime 5 type. Thus it could seem likely that the high frequency or primary oscillation noted here can be identified with Schwind's regime 5 and the low frequency or secondary oscillation with Schwind's regime 4. Schwind observed that in general regime 5 oscillations occur at higher speeds than regime 4 oscillations (although they could both occur at the same speed). This agrees well with the results presented here where the primary oscillations persist to much higher values of UD/ν than do the secondary oscillations.

The above describes the oscillatory behaviour of the horseshoe vortex oscillations.

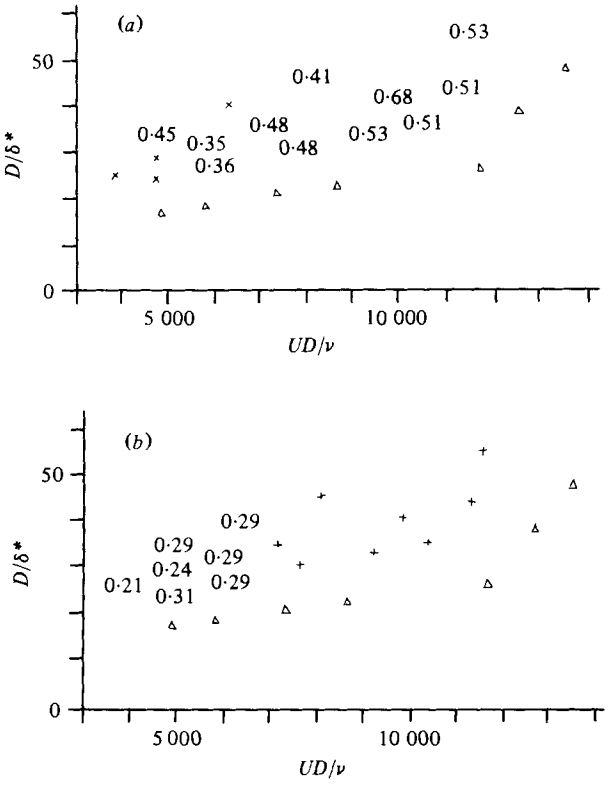

FIGURE 14. Variation of vortex oscillation frequencies: (*a*) primary oscillations; (*b*) secondary oscillations. Numbers indicate values of St; + indicates that only primary oscillations were visible; × indicates that only secondary oscillations were visible; △ indicates that no regular oscillations were visible.

However, it does not explain what causes these oscillations. One can, however, eliminate some possible causes. To test whether the wake vortex shedding of the cylinder had any effect on the oscillations, tests were carried out with a cylinder with splitter plate and with a streamlined model, for both of which the wake spectrum was found to be significantly different from that of the cylinder. Results almost identical to those described above were obtained. Also it can be seen from figure 15(*a*) that the Strouhal number for the wake vortex shedding of the cylinder is approximately 0·16 at all tunnel speeds, which bears no relationship to the observed frequencies of oscillation of the horseshoe vortex systems. Thus it appears that one can eliminate wake vortex shedding as a possible cause of the oscillations.

Figure 15(*b*) shows the speed of rotation of the wind tunnel fan non-dimensionalized using the cylinder diameter and the wind-tunnel freestream velocity, plotted against a Reynolds number based on cylinder diameter. Again the Strouhal number bears no relationship to the Strouhal number of the vortex oscillations. In fact this Strouhal number decreases with Reynolds number while the Strouhal number of the vortex oscillations increases with Reynolds number. So it would appear that these oscillations are not affected by any disturbances caused by the fan.

Now consider the spectrum shown in figure 15(*c*). This shows the spectrum recorded in the boundary layer on the wind-tunnel wall downstream of the suction slot, at the

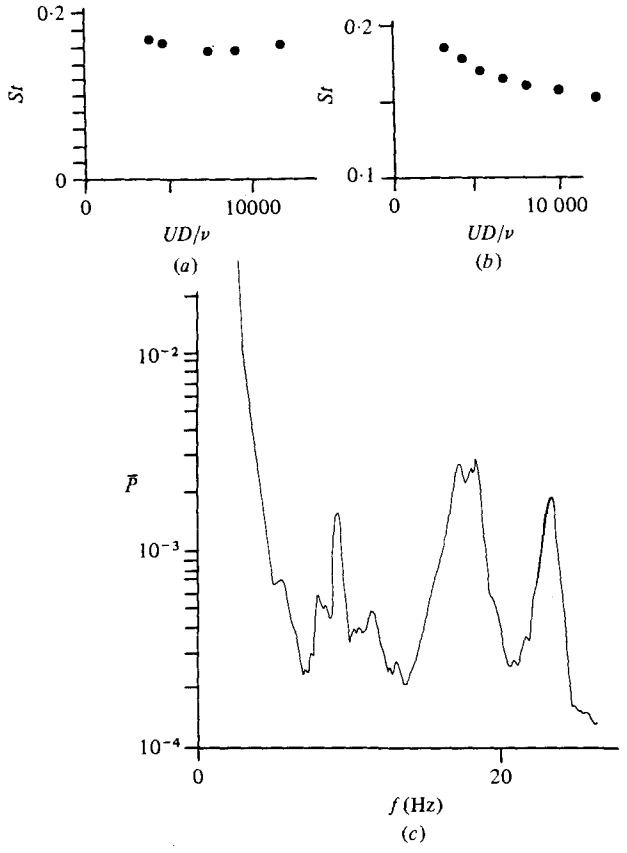

FIGURE 15. Sources of disturbance in wind tunnel: (*a*) cylinder vortex shedding; (*b*) variation in fan speed; (*c*) undisturbed boundary-layer spectrum. ($UD/\nu = 4750$, $D/\delta^* = 34{\cdot}0$, $y/D = 0{\cdot}063$.)

same flow conditions as for figure 10 but with the cylinder not in position. The spectrum shows a large d.c. peak together with several other peaks. However, these peaks do not correspond to either of the horseshoe vortex oscillation frequencies at this speed. In fact two of the dominant peaks on this spectrum, the ones at 9·4 and 18·8 Hz, do not change their position as the tunnel speed varies. This would suggest that they are related to an oscillation frequency of the wind-tunnel structure. So it would appear that any disturbances present in the boundary-layer upstream of the model do not affect the horseshoe vortex oscillations.

Thus having eliminated all the above possibilities for the case of vortex oscillations the author can see only one explanation for these oscillations; that is, at certain values of UD/ν and D/δ^* the horseshoe vortex itself becomes unstable for some reason, and begins to oscillate in one of two 'natural' modes, the higher frequency mode becoming more dominant as the Reynolds number increases.

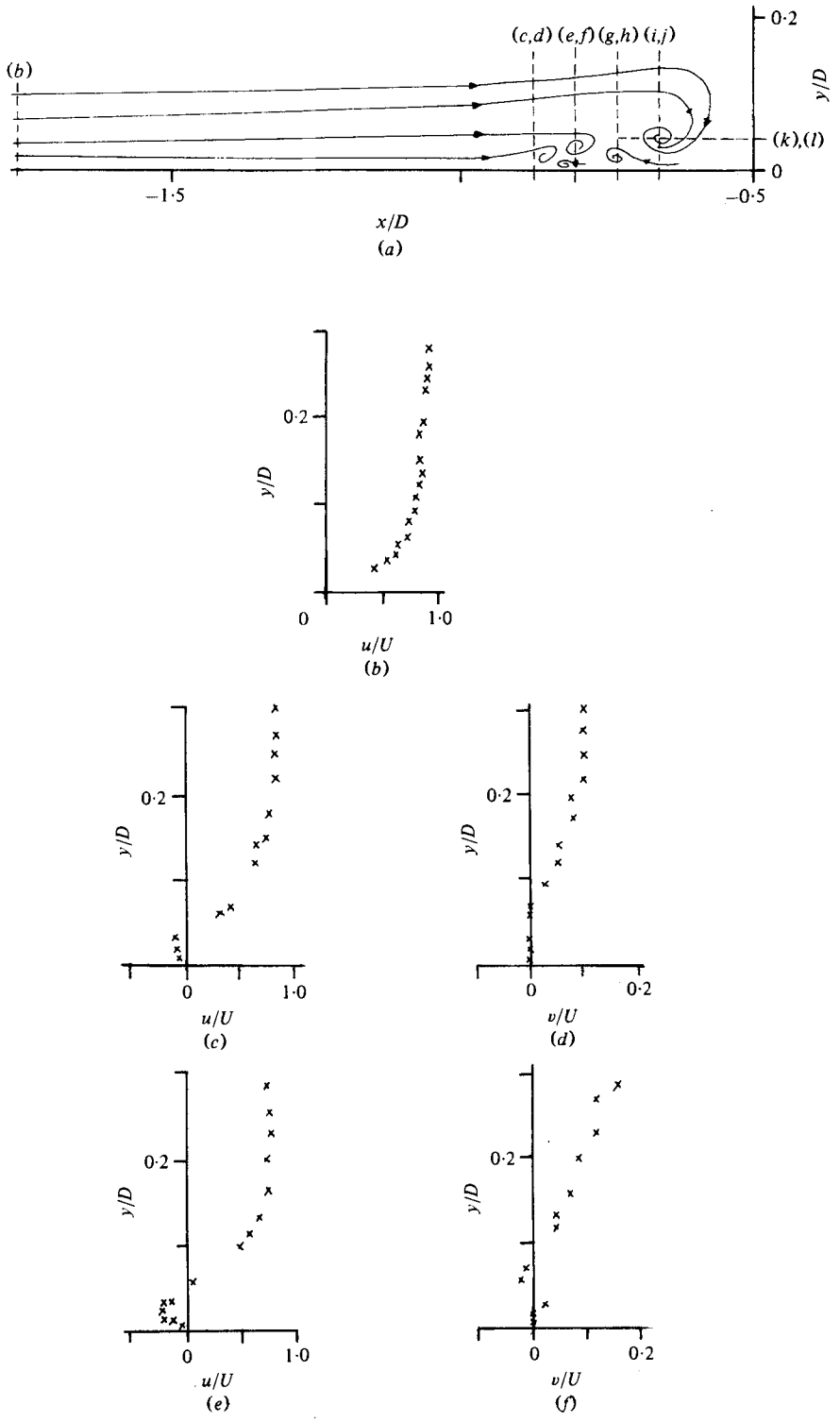

FIGURE 16 (*a–f*). For caption see next page.

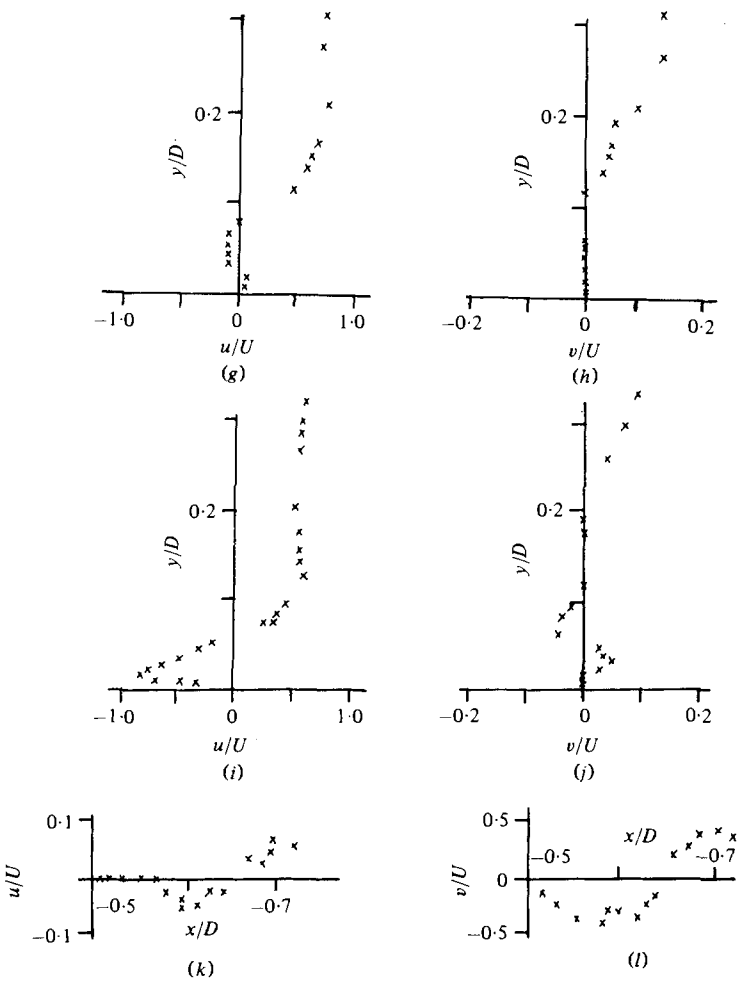

FIGURE 16. Velocity profiles ($UD/\nu = 2610$, $D/\delta^* = 14{\cdot}8$). (*a*) The positions of the profiles (*b*)–(*l*). (*b*) $x/D = -1{\cdot}75$; (*c*, *d*) $x/D = -0{\cdot}87$; (*e*, *f*) $x/D = -0{\cdot}79$; (*g*, *h*) $x/D = -0{\cdot}73$; (*i*, *j*) $x/D = -0{\cdot}66$; (*k*, *l*) $y/D = 0{\cdot}06$.

8. Velocity measurements in the smoke tunnel

Velocity measurements on the plane of symmetry upstream of a cylinder in the smoke tunnel are shown in figure 16, for $UD/\nu = 2610$, $D/\delta^* = 14{\cdot}8$. The sections for which velocity profiles are presented are shown in figure 16 (*a*). The velocity profile in a direction parallel to the plate for a section perpendicular to the plate, upstream of the vortex system, is shown in figure 16 (*b*). Velocity profiles in directions parallel and perpendicular to the plate at a section perpendicular to the plate just downstream of the separation point are shown in figure 16 (*c*) and (*d*) respectively; similar profiles through vortex 2 are shown in figure 16 (*e*) and (*f*); through vortex 1′ in figure 16 (*g*) and (*h*); and through vortex 1 in figure 16 (*i*) and (*j*). The velocity profiles in directions parallel and perpendicular to the plate for a section through the centre of vortex 1 parallel to the plate are shown in figure 16 (*k*) and (*l*). The reversed flow within the vortex systems can be plainly seen in these figures. The expected double crossover in

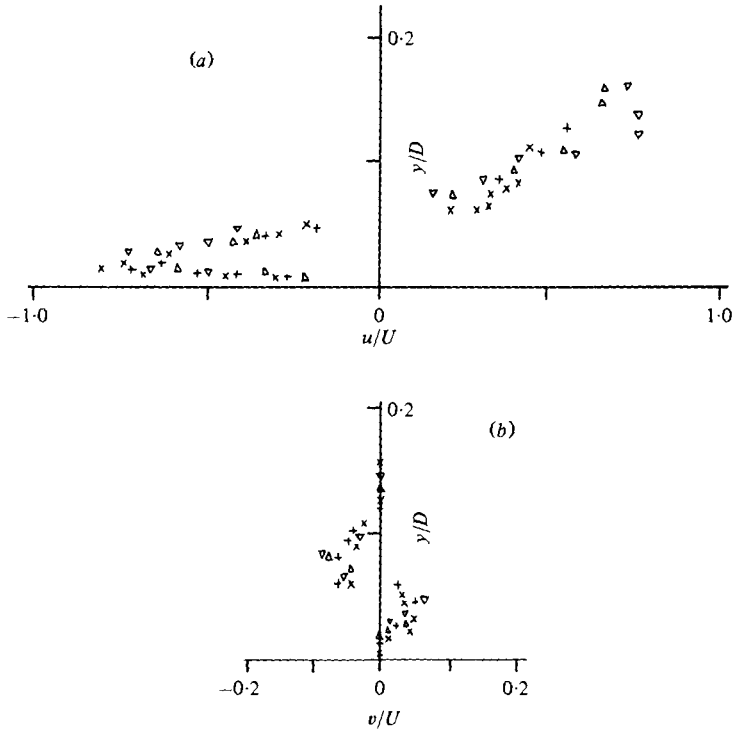

FIGURE 17. Velocity profiles through vortex *l* at several speeds. (*a*) u/U versus y/D; (*b*) v/U versus y/D. ×, $UD/\nu = 2610$, $D/\delta^* = 14{\cdot}8$, $x/D = -0{\cdot}66$; +, $UD/\nu = 3100$, $D/\delta^* = 16{\cdot}1$, $x/D = -0{\cdot}67$; △, $UD/\nu = 3600$, $D/\delta^* = 17{\cdot}3$, $x/D = -0{\cdot}68$; ▽, $UD/\nu = 4240$, $D/\delta^* = 18{\cdot}8$, $x/D = -0{\cdot}69$. Error in $u/U \approx \pm 0{\cdot}05$; error in $v/U \approx \pm 0{\cdot}05$.

the velocity profile can also be seen in figure 16(*g*). Here the flow in vortex 1′ is in the downstream direction close to the plate, in the upstream direction away from the wall, and in the downstream direction out of the vortex system.

For the velocity profiles through vortices 2, 1′ and 1 (figure 16(*e*), (*f*), 16(*g*), (*h*) and 16(*i*), (*j*) respectively) it will be appreciated that the velocity components parallel to and perpendicular to the plate are equivalent to the vortex circumferential and radial velocity components respectively. Within the vortex system a significant vortex radial flow component can only be measured within vortices 1 and 2. The radial component of velocity can be seen to be an order of magnitude smaller than the circumferential component.

Within the cores of the vortices the radial flow component was measured in two ways: by resolving the flow velocity at the measurement sections in a radial direction, and by measuring the variation of the distance of a streamline from the vortex centre between two successive crossings by the streamline of the measurement section. The latter method effectively gives a mean radial velocity for half a streamline spiral around the vortex. However, these methods gave more or less identical results close to the centre of the vortices.

Figure 17 shows velocity profiles in directions perpendicular and parallel to the plate, for a section perpendicular to the plate, through the centre of vortex 1 at four different speeds. This figure shows that the non-dimensional velocity profiles do not

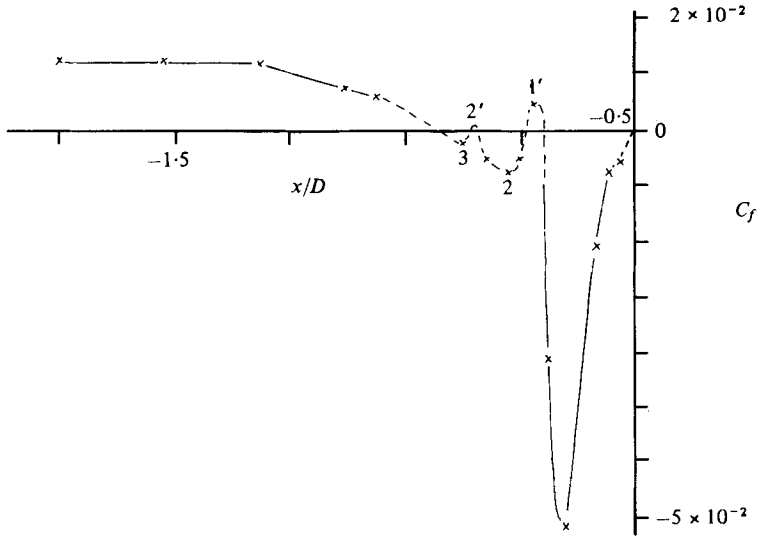

FIGURE 18. Skin friction beneath a horseshoe vortex system ($UD/\nu = 2610$, $D/\delta^* = 14{\cdot}8$).

vary greatly in and beneath the vortex core. Any variation may, however, be obscured by the rather large errors indicated. Above the vortex core, however, the horizontal velocity profiles do vary with the flow parameters. This is because as UD/ν increases vortex 1 moves away from the cylinder to a position where the dimensionless velocity outside the vortex system is higher.

Finally in figure 18 the distribution of skin friction beneath the horseshoe vortex system is shown. The data presented in this figure was taken from the velocity profiles of figure 16 and other velocity profiles. The dotted lines in the figure indicate a region where the skin friction could not be measured, such as near a separation or attachment point, but where its variation could be deduced, i.e. $|C_f|$ must fall to zero at such a point. The most striking feature of this figure is the high value of $|C_f|$ beneath vortex 1, approximately five times the freestream value upstream of the vortex system. Beneath vortex 2, the value of $|C_f|$ is somewhat less than the upstream value, and beneath vortex 3 it is much less. Thus although over much of the vortex system on the plane of symmetry there is a reduction in $|C_f|$ from its freestream value, there is a considerable increase in $|C_f|$ beneath vortex 1.

9. Conclusions

(*a*) The horseshoe vortex upstream of a cylinder in a laminar boundary layer has been visualized using smoke flow visualization. Three different types of vortex system have been observed which are, with increasing UD/ν:

(i) steady horseshoe vortex systems with 2, 4 or 6 vortices, the number of vortices increasing as UD/ν increases;

(ii) horseshoe vortex systems which exhibit a regular oscillatory motion;

(iii) horseshoe vortex systems which exhibit an irregular unsteady behaviour.

(*b*) Pressure distributions were measured on the plane of symmetry upstream of models of various types over a wide range of flow conditions ($2000 < UD/\nu < 16\,000$, $20 < D/\delta^* < 70$). Two types of pressure distribution were measured.

(i) Pressure distributions which show minima. Flow visualization shows that such minima are at the position of the horseshoe vortex. Thus the vortex position can be determined from such pressure distributions.

(ii) Pressure distributions which show no minima. Flow visualization shows that this type of pressure distribution occurs when the horseshoe vortex systems are unsteady.

(*c*) The variation of the position of the primary horseshoe vortex in steady vortex systems, as UD/ν and D/δ^* vary, has been presented in a graphical form. $|x_v/D|$ increases as UD/ν increases and as D/δ^* decreases. A theoretical analysis which predicts the position of the separation line upstream of a circular cylinder on a plate, suggests that the horseshoe vortex position is not solely determined by this separation position but some other effect plays a part.

(*d*) The oscillatory behaviour of horseshoe vortex systems was found to be complex. As the Reynolds number UD/ν increased steady horseshoe vortex systems began to oscillate intermittently and randomly at two different frequencies. As UD/ν increased further the periods of oscillation became longer, the high frequency oscillation becoming more common. At yet higher UD/ν the oscillations became irregular and the horseshoe vortex system became turbulent. These oscillations are not caused by vortex shedding in the wake of the models or by any small disturbances within the wind tunnel. It is concluded that the frequency of these oscillations is solely determined by the values of UD/ν and D/δ^*.

(*e*) The velocity distributions within steady laminar horseshoe vortex systems have been measured using smoke flow visualization. A radial flow component can be measured only in vortices 1 and 2, and appears to increase linearly with the distance from the centre of the vortex, in the central region of the vortex. There was found to be little variation in the dimensionless velocity profiles, within the vortex system, as the flow speed varied, although any variation may well have been obscured by the rather large measurement errors.

(*f*) The skin friction coefficient beneath vortex 1 was found to have a numerical value of five times its value far upstream of the cylinder, for $UD/\nu = 2610$, $D/\delta^* = 14{\cdot}8$.

The author wishes to acknowledge the help and advice of Mr E. P. Sutton, his thesis supervisor. The author was in receipt of a maintenance grant from the Science Research Council during the course of the experimental investigation.

REFERENCES

BAKER, C. J. 1978 Vortex flow around the bases of obstacles. Ph.D. thesis, University of Cambridge.

SCHWIND, R. 1962 The three-dimensional boundary layer near a strut. *Gas Turbine Lab. Rep.*, MIT.

TIMMAN, R. 1955 The theory of three-dimensional boundary layers. In *Symp. on Boundary Layer Effects in Aerodyn.* NPL.

THWAITES, B. 1960 *Incompressible Aerodynamics.* Oxford University Press.

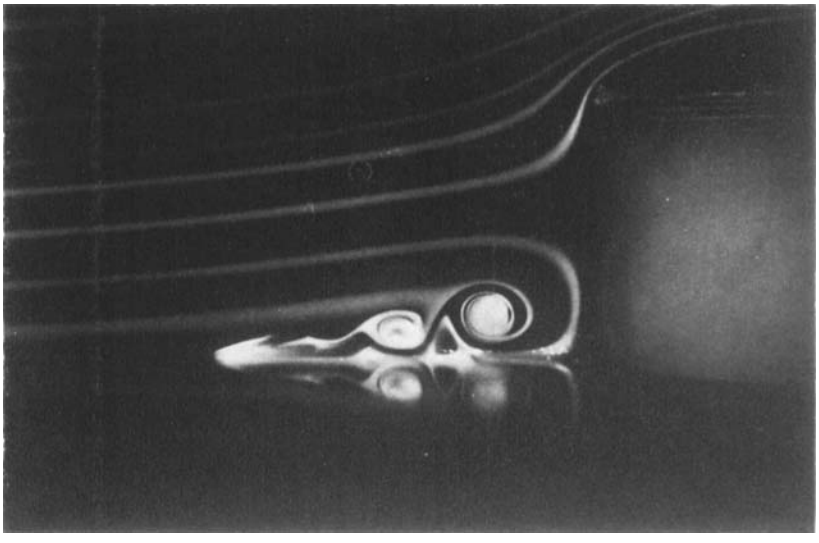

FIGURE 1. Sutton's experiment.

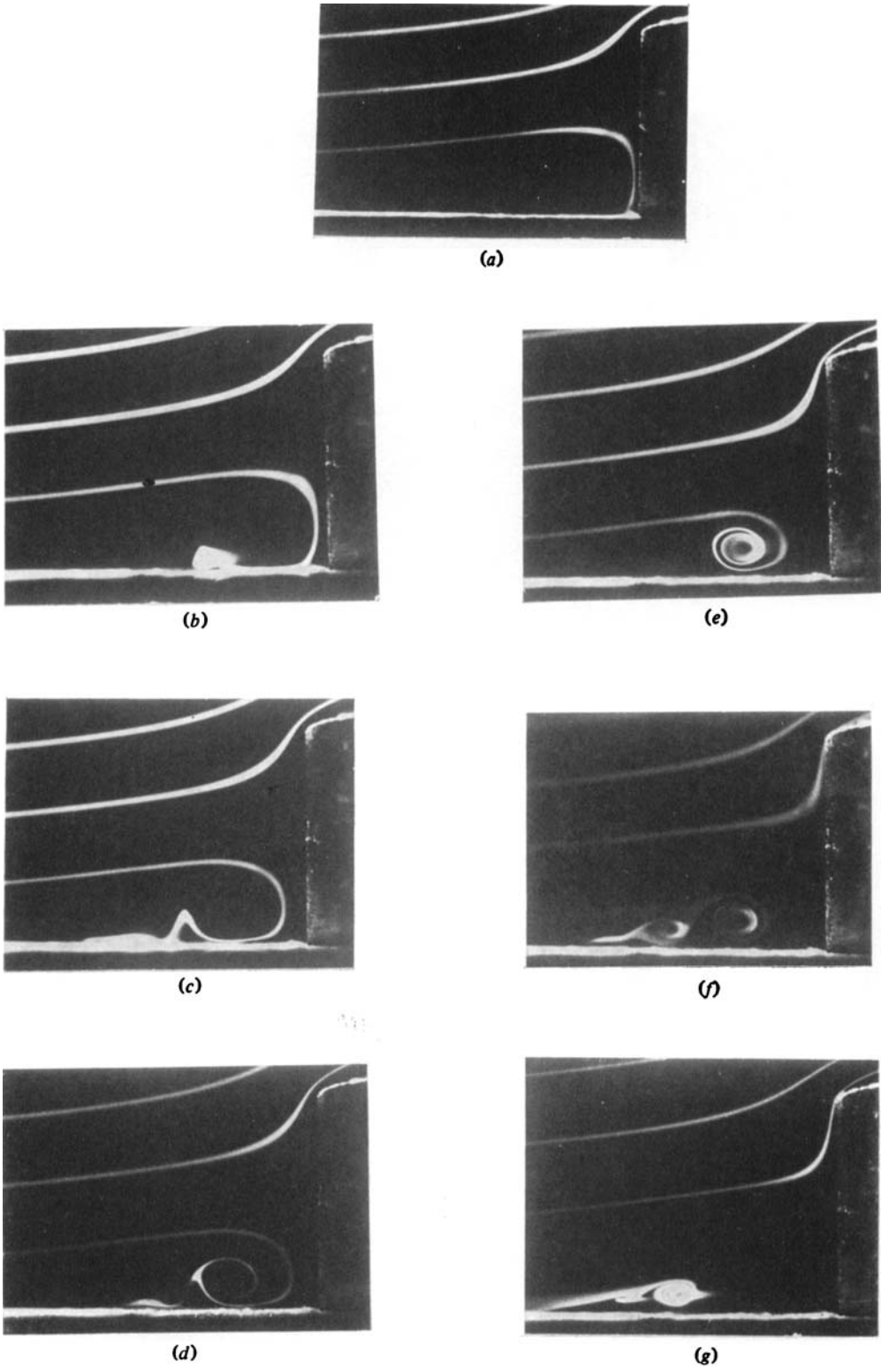

FIGURE 4. Smoke flow visualization ($UD/\nu = 4370$, $D/\delta^* = 21{\cdot}3$, $D/l = 2{\cdot}0$).

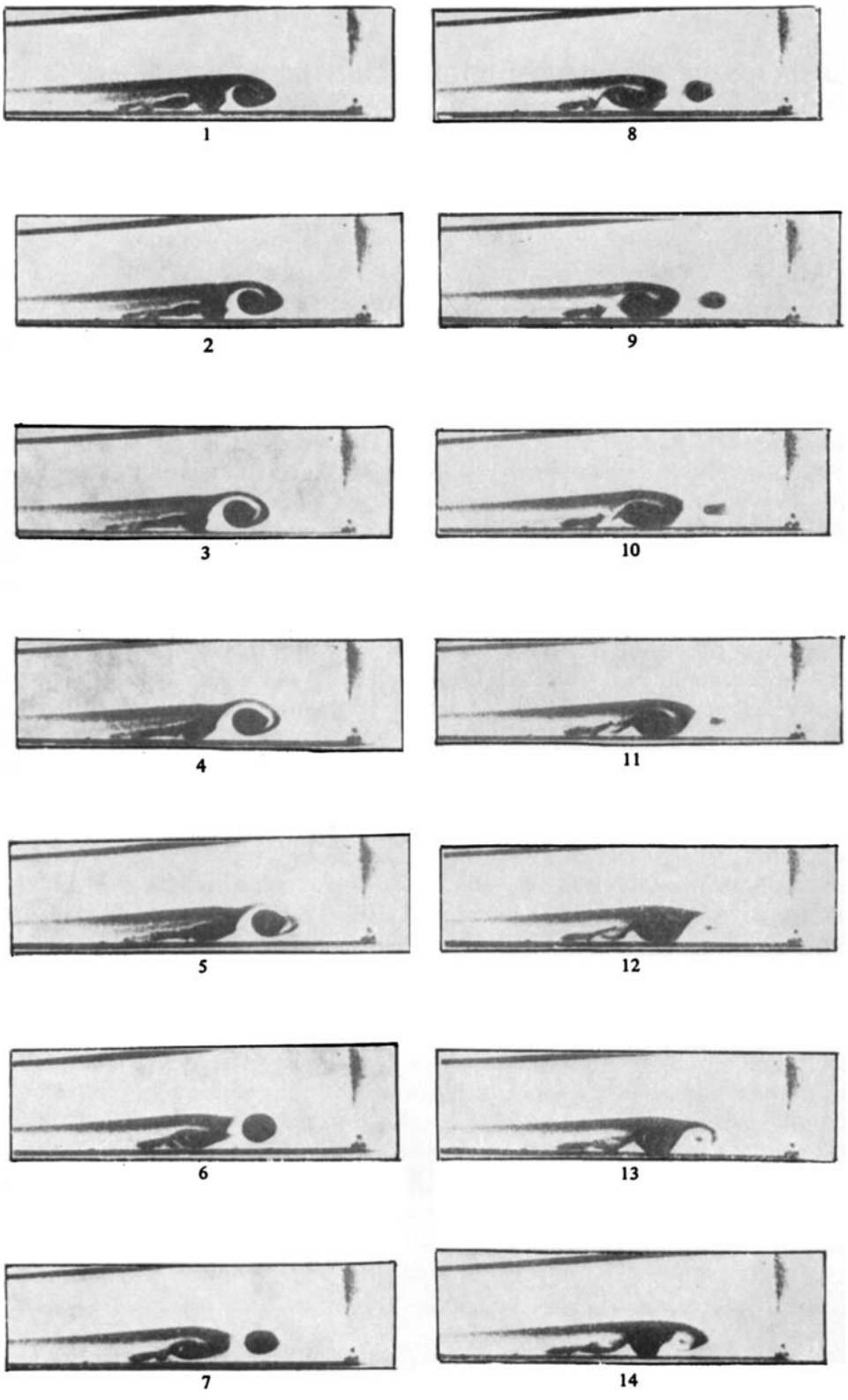

FIGURE 7. Oscillating vortex system ($UD/\nu = 5200$, $D/\delta^* = 23{\cdot}2$, $D/l = 2{\cdot}0$).